Inorganic Chemistry
Article

Inorg. Chem. **2010**, *49*, 11045–11056 **11045**
DOI: 10.1021/ic1015725

Dimensionality Switching Through a Thermally Induced Reversible Single-Crystal-to-Single-Crystal Phase Transition in a Cyanide Complex

Ruxandra Gheorghe,[†] Marguerite Kalisz,[‡,§] Rodolphe Clérac,[‡,§] Corine Mathonière,[∥] Patrick Herson,[⊥] Yanling Li,[⊥] Mannan Seuleiman,[⊥] Rodrigue Lescouëzec,[*,⊥] Francesc Lloret,[#] and Miguel Julve[*,#]

[†]*Inorganic Chemistry Laboratory, Faculty of Chemistry, University of Bucharest, str. Dumbrava Rosie 23, 020464 Bucharest, Romania,* [‡]*CNRS, UPR 8641, Centre de Recherche Paul Pascal (CRPP), Equipe "Matériaux Moléculaires Magnétiques", 115 avenue du Dr. Albert Schweitzer, Pessac, F-33600, France,* [§]*Université de Bordeaux, UPR 8641, Pessac, F-33600, France,* [∥]*CNRS, Institut de Chimie de la Matière Condensée de Bordeaux UPR 9048, Université de Bordeaux, 87 av. Dr. Schweitzer, 33600 Pessac,* [⊥]*Institut Parisien de Chimie Moléculaire, UMR7201, Université Paris 6, 4 place Jussieu, F-75252 Paris, Cedex 05, France, and* [#]*Departament de Química Inorgánica/Instituto de Ciencia Molecular, Universitat de València, C/José Beltrán 2, 46980 Paterna (València), Spain.*

Received August 4, 2010

The heterometallic hexanuclear cyanide-bridged complex $\{[Mn(bpym)(H_2O)]_2[Fe(HB(pz)_3)(CN)_3]_4\}$ (**1**), its $C^{15}N$ and D_2O enriched forms $\{[Mn(bpym)(H_2O)]_2[Fe(HB(pz)_3)(C^{15}N)_3]_4\}$ (**2**) and $\{[Mn(bpym)(D_2O)]_2[Fe(HB(pz)_3)(CN)_3]_4\}$ (**3**), and the hexanuclear derivative complex $\{[Mn(bpym)(H_2O)]_2[Fe(B(pz)_4)(CN)_3]_4\}\cdot 4H_2O$ (**4**) [bpym = 2,2′-bipyrimidine, $HB(pz)_3^-$ = hydrotris(1-pyrazolyl)borate, $B(pz)_4^-$ = tetra(1-pyrazolyl)borate] have been synthesized. Their structures have been determined through single-crystal X-ray crystallography at different temperatures. Whereas **3** and **4** maintain a discrete hexanuclear motif during the entire temperature range investigated (down to 95 K), **1** and **2** exhibit a thermally induced reversible single-crystal to single-crystal phase transition driven by a remarkable concerted rearrangement of hydrogen and cyanide coordination bonds. While hexanuclear complexes are observed in the high temperature phases (noted **1a** and **2a**) above 200 K, the low temperature phases are composed of one-dimensional coordination polymers noted **1b** and **2b**. The magnetic properties of the four compounds have been investigated in the 2−300 K range, and they reveal the occurrence of an overall antiferromagnetic behavior. The thermal dependence of the optical reflectivity and the FT-IR absorbance have been studied for **1** in the range 10−300 K and 130−300 K, respectively. A comparative analysis of the structural and electronic properties for **1**−**4** clearly underlines the major role of the intermolecular interactions in the topological and dimensional rearrangement observed during the structural phase transition. This result opens new perspectives in the design of cyanide-based switchable magnetic materials using coordination bonds rearrangements.

Introduction

The cyanide group is one of the simplest metal linkers that can be used to design molecule-based materials. Its ambidentate character makes it suitable to selectively connect two different metal ions forming a quasi linear M−CN−M′ motif allowing a fairly good prediction of the topologies of the resulting compounds.[1] The Prussian blue analogues (PBAs) are probably the most famous compounds ever made with the cyanide ligand. They are three-dimensional coordination polymers of general formula $[A_xM_y\{M'(CN)_6\}_z]$ in which the cyanide groups act as bridges between six-coordinate transition metal ions M and M′ (A is an optional alkali metal ion). Three hundred years after the accidental discovery of the original Prussian blue $[Fe^{III}_4\{Fe^{II}(CN)_6\}_3]$ (ferric ferrocyanide), impressive research efforts are still devoted to explore the always reviving potential of these materials. Recent publications involve a wide range of applications including hydrogen gas storage,[2] waste recovering,[3] (bio)sensors,[4] or heterogeneous catalysis.[5] The cyanide ligand is also an efficient mediator of

*To whom correspondence should be addressed. E-mail: rodrigue.lescouezec@upmc.fr (R.L.), miguel.julve@uv.es (M.J.).

(1) Dunbar, K. R.; Heintz, R. A. *Prog. Inorg. Chem.* **2007**, *45*, 283.

(2) (a) Kaye, S. S.; Long, J. R. *J. Am. Chem. Soc.* **2005**, *127*, 6506. (b) Chapman, K. W.; Southon, P. D.; Weeks, C. L.; Kepert, C. J. *Chem. Commun.* **2005**, 3322. (c) Reguera, L.; Krap, C. P.; Balmaseda, J.; Reguera, E. *J. Phys. Chem. C* **2008**, *112*, 15893. (d) Thallapally, P. K.; Motkuri, R. K.; Fernandez, C. A.; McGrail, B. P.; Behrooz, G. S. *Inorg. Chem.* **2010**, *49*, 4909.

(3) Valentini, M. T. G.; Stella, R.; Maggi, L.; Ciceri, G. *J. Radioanal. Nucl. Chem.* **1987**, *114*, 105.

(4) Koncki, R. *Crit. Rev. Anal. Chem.* **2002**, *32*, 79.

(5) (a) Karyakin, A.; Karyakina, E.; Gorton, L. *Anal. Chem.* **2000**, *72*, 1720. (b) Kumar, A. S.; Zen, J. M. *ChemPhysChem* **2004**, *5*, 1227.

Published on Web 10/27/2010

magnetic interactions when acting as a bridge between paramagnetic centers. Besides from being suitable candidates to test theoretical models describing the magnetic interactions,[6] the corresponding PBA-like phases display often magnet-type properties with adjustable values of the ordering temperature.[7] Recently, the discovery of examples of single-molecule (SMM) and single-chain (SCM) magnets in low-dimensional magnetic cyanide-based systems has enhanced the interest in this field of research. As these SMMs and SCMs display slow relaxation of their magnetization (i.e., a magnet-type behavior) at low temperatures, it has been suggested that they could be used as molecular magnetic memories for information storage.[8] Within this context, we have explored the use of tailored cyanide-bearing building blocks containing a reduced number of cyanide ligands to promote low-dimensional structural arrangements.[9] This approach has been successful, and some cyanide-based nanomagnets have been recently published.[10,11] When looking for potential applications, the most interesting systems are probably those implying a switch of the physical properties via an external physical or chemical stimulus. For example, Long et al. have recently published a redox switchable SMM.[12] Indeed, switchable systems are an important topic in materials science and in particular in the cyanide chemistry, an area that offers many examples of such materials, whatever their dimensionality could be. A variety of external stimuli such as temperature,[13] pressure,[14] redox,[15] light excitation,[16] or gas adsorption,[17] have proved to be efficient in inducing electronic changes (e.g., charge transfer and/or spin state conversion) and consequently, in causing significant modifications of the magnetic behavior. Interestingly, physical properties may also be tuned through structural reorganization of the material induced by an order−disorder transition or solvent absorption/desorption. For example, Kitagawa et al. recently reported the synthesis of a cyanide-based magnet that displays a reversible change in its structural dimensionality between a two- and a three-dimensional coordination network upon solvent absorption/desorption.[18] This structural reorganization implies a modification of the magnetic ions connectivity, that is, a bridging cyanide ligand is reversibly replaced by a solvent molecule, and therefore a significant shift of the Curie temperature occurs. This type of behavior known as a "topo-chemical reaction" is rarely observed directly, as it requires single crystal diffraction studies in both crystalline phases. Unfortunately, single-crystal X-ray diffraction is particularly difficult in such systems because of the crystallinity loss that is usual over the topological reorganization.[19] We report herein a new thermally induced topo-chemical reaction associated with a dimensionality switching in the heterometallic hexanuclear cyanide-based complex $\{[Mn(bpym)(H_2O)]_2[Fe(HB(pz)_3)(CN)_3]_4\}$ (**1**) [bpym = 2,2′-bipyrimidine and $HB(pz)_3^-$ = hydrotris(1-pyrazolyl)borate]. This compound exhibits a reversible single-crystal-to-single-crystal (SCSC) structural phase transition around 200 K through a concerted reorganization of coordination and hydrogen bonds. The starting hexanuclear molecular complex **1a** is converted into an one-dimensional (1D) coordination polymer **1b**. In contrast to previously reported topo-chemical reactions,[18,20] here the dimensionality switch does not involve a solvent absorption/desorption phenomenon. While the SCSC transition has also been observed around 200 K in the $C^{15}N$ enriched compound, $\{[Mn(bpym)(H_2O)]_2[Fe(HB(pz)_3)(C^{15}N)_3]_4\}\cdot$ (**2**), the D_2O enriched sample $\{[Mn(bpym)(D_2O)]_2[Fe(HB(pz)_3)(CN)_3]_4\}$ (**3**), and the hexanuclear complex $\{[Mn(bpym)(H_2O)]_2[Fe(B(pz)_4)(CN)_3]_4\}\cdot 4H_2O$ (**4**) [$B(pz)_4^-$ = tetra(1-pyrazolyl)borate] (the last one containing a bulkier blocking ligand on the iron centers) maintain their hexanuclear topology over the investigated temperature range (95−300 K). The comparative structural investigations of the four compounds clearly support the

(6) (a) Verdaguer, M.; Bleuzen, A.; Train, C.; Garde, R.; Debiani, F. F.; Desplanches, C. *Philos. Trans. R. Soc. London. Ser. A* **1999**, *357*, 2959. (b) Ruiz, E.; Rodriguez-Fortea, A.; Alvarez, S.; Verdaguer, M. *Chem.—Eur. J.* **2005**, *11*, 2135.

(7) (a) Verdaguer, M.; Bleuzen, A.; Marvaud, V.; Vaissermann, J.; M. Seuleiman, M.; Desplanches, C.; Scuiller, A.; Train, C.; Garde, R.; Gelly, G.; C. Lomenech, C.; Rosenman, I.; Veillet, P.; Cartier dit Moulin, C.; Villain, F. *Coord. Chem. Rev.* **1999**, *190*, 1023. (b) Ferlay, S.; Mallah, T.; R. Ouahès, R.; Veillet, P.; Verdaguer, M. *Nature* **1995**, *378*, 701. (c) Holmes, S. M.; Girolami, G. S. *J. Am. Chem. Soc.* **1999**, *121*, 5593.

(8) (a) Long, J. R. Molecular Cluster Magnets. In *Chemistry of Nanostructured Materials*; Yang, P., Ed.; World Scientific: Hong Kong, 2003; pp 291−315 and references therein. (b) Gatteschi, D.; Sessoli, R.; Villain, J. *Molecular Nanomagnets*; Oxford University Press: New York, 2006 and references therein. (c) Wernsdorfer, W.; Aliaga-Alcalde, N.; Hendrickson, D. N.; Christou, G. *Nature* **2002**, *416*, 406. (d) Leuenberger, M.; Loss, D. *Nature* **2001**, *410*, 789. (e) Gatteschi, D.; Sessoli, R. *Angew. Chem., Int. Ed.*, **2003**, *42*, 268 and references therein.

(9) (a) Lescouëzec, R.; Vaisermann, J.; Toma, L. M.; Carrasco, R.; Lloret, F.; Julve, M. *Inorg. Chem.* **2004**, *43*, 2234. (b) Lescouëzec, R.; Lloret, F.; Julve, M.; Vaissermann, J.; Verdaguer, M. *Inorg. Chem.* **2002**, *41*, 5943. (c) Lescouëzec, R.; Toma, L. M.; Vaissermann, J.; Verdaguer, M.; Delgado, F. S.; Ruiz-Pérez, C.; Lloret, F.; Julve, M. *Coord. Chem. Rev.* **2005**, *249*, 2691.

(10) See for exemple: (a) Sokol, J. J.; Hee, A. G.; Long, J. R. *J. Am. Chem. Soc.* **2002**, *124*, 7656–7657. (b) Berlinguette, C. P.; Vaughn, D.; Canada-Vilalta, C.; Gálan-Mascarós, J. R.; Dunbar, K. R. *Angew. Chem., Int. Ed.* **2003**, *42*, 1523–1526. (c) Beltran, L. M. C.; Long, J. R. *Acc. Chem. Res.* **2005**, *38*, 325–334. (d) Li, D.; Parkin, S.; Wang, G.; Yee, G. T.; Clérac, R.; Wernsdorfer, W.; Holmes, S. M. *J. Am. Chem. Soc.* **2006**, *128*, 4214–4215.

(11) See for example: (a) Lescouëzec, R.; Vaissermann, J.; Ruiz-Pérez, C.; Lloret, F.; Carrasco, R.; Julve, M.; Verdaguer, M.; Dromzée, Y.; Gatteschi, D.; Wernsdorfer, W. *Angew. Chem., Int. Ed.* **2003**, *42*, 1483. (b) Wang, S.; Zuo, J.-L.; Gao, S.; Song, Y.; Zhou, H.-C.; Zhang, Y.-Z.; You, X.-Z. *J. Am. Chem. Soc.* **2004**, *126*, 8900. (c) Ferbinteanu, M.; Miyasaka, H.; Wernsdorfer, W.; Nakata, K.; Sugiura, K.; Yamashita, M.; Coulon, C.; Clérac, R. *J. Am. Chem. Soc.* **2005**, *127*, 3090–3099. (d) Toma, L. M.; Lescouëzec, R.; Pasán, J.; Ruiz-Pérez, C.; Vaissermann, J.; Cano, J.; Carrasco, R.; Wernsdorfer, W.; Lloret, F.; Julve, M. *J. Am. Chem. Soc.* **2006**, *128*, 4842. (e) Harris, T. D.; Bennett, M. V.; Clérac, R.; Long, J. R. *J. Am. Chem. Soc.* **2010**, *132*, 3980. (f) Venkatakrishnan, T. S.; Sahoo, S.; Bréfuel, N.; Duhayon, C.; Paulsen, C.; Barra, A.-L.; Ramasesha, S.; Sutter, J. P. *J. Am. Chem. Soc.* **2010**, *132*, 6047–6056.

(12) Freedman, D. E.; Jenkins, D. M.; Iavarone, A. T.; Long, J. R. *J. Am. Chem. Soc.* **2008**, *130*, 2884–2885.

(13) (a) Ohkoshi, S.-I.; Matsuda, T.; Tokoro, H.; Hashimoto, K. *Chem. Mater.* **2005**, *17*, 81. (b) Niel, V.; Martinez-Agudo, J. M.; Muñoz, M. C.; Gaspar, A. B.; Real, J. A. *Inorg. Chem.* **2001**, *40*, 3838.

(14) (a) Morimoto, Y.; Hanawa, M.; Ohiski, Y.; Kato, K.; Takata, M.; Kuriki, A.; Nishibori, E.; Sakata, M.; Ohkoshi, S.; Tokoro, H.; Hashimoto, K. *Phys. Rev. B* **2003**, *68*, 144106. (b) Real, J. A.; Galet, A.; Gaspar, A. B.; Agusti, G.; Munoz, M. C. *Chem. Phys. Lett.* **2006**, *434*, 68.

(15) Sato, O.; Iyoda, T.; Fujishima, A.; Hashimoto, K. *Science* **1996**, *271*, 49.

(16) See for example: (a) Verdaguer, M. *Science* **1996**, *272*, 698. (b) Ohkoshi, S.-i.; Ikeda, S.; Hozumi, T.; Kashiwagi, T.; Hashimoto, K. *J. Am. Chem. Soc.* **2006**, *128*, 5320. (c) Sato, O.; Tao, J.; Zhang, Y.-Z. *Angew. Chem., Int. Ed.* **2007**, *46*, 2152. (d) Li, D.; Clérac, R.; Roubeau, O.; Harte, E.; Mathonière, C.; Le Bris, R.; Holmes, S. M. *J. Am. Chem. Soc.* **2008**, *130*, 252. (e) Bleuzen, A.; Marvaud, V.; Mathonière, C.; Sieklucka, B.; Verdaguer, M. *Inorg. Chem.* **2009**, *48*, 3453.

(17) Kaye, S. S.; Jin Choi, H.; Long, J. R. *J. Am. Chem. Soc.* **2008**, *130*, 16921.

(18) Kaneko, W.; Ohba, M.; Kitagawa, S. *J. Am. Chem. Soc.* **2007**, *129*, 13706.

(19) Vittal, J. J. *Coord. Chem. Rev.* **2007**, *251*, 1781.

(20) See for example: (a) Mukherjee, P. S.; Lopez, N.; Arif, A. M.; Cervantes-Lee, F.; Noveron, J. C. *Chem. Commun.* **2007**, 1433. (b) Campo, J.; Falvello, L. R.; Mayoral, I.; Palacio, F.; Soler, T.; Toms, M. *J. Am. Chem. Soc.* **2008**, *130*, 2932. (c) Zhang, Y.-J.; Liu, T.; Kanegawa, S.; Sato, O. *J. Am. Chem. Soc.* **2009**, *131*, 7942. (d) Zhang, Y.-J.; Liu, T.; Kanegawa, S.; Sato, O. *J. Am. Chem. Soc.* **2009**, *132*, 912.

Table 1. Unit Cell Parameters of **1**−**4**

	compound, T(K)						
	1a, *295(2)*	**1b**, *200(2)*	**2a**, *295(2)*	**2b**, *200(2)*	**3**, *295(2)*	**3**, *200(2)*	**4**, *200(2)*
a (Å)	8.804(1)	15.419(2)	8.817(2)	15.428(1)	8.809(1)	8.790(2)	8.856(2)
b (Å)	15.207(2)	8.832(2)	15.242(2)	8.835(1)	15.212(2)	15.213(5)	15.672(2)
c (Å)	16.000(2)	29.855(5)	16.032(1)	29.861(5)	16.026(3)	15.944(4)	18.221(3)
α (deg)	86.38(1)	90	86.34(1)	90	86.46(1)	86.76(2)	88.99(1)
β (deg)	87.56(1)	91.82(1)	87.64(1)	91.83(1)	87.42(1)	87.56(2)	89.98(1)
γ (deg)	75.26(1)	90	75.24(1)	90	75.25(1)	75.35(2)	74.18(1)
V (Å^3)	2066.6(5)	4063.6(10)	2078.5(5)	4068.1(10)	2071.7(6)	2058.6(10)	2432.8(8)

importance of the intermolecular interactions, and more precisely, the key role of the hydrogen bonds in the topological rearrangement. In addition, the physical properties of **1** have been studied by IR spectroscopy, surface optical reflectivity, and magnetic susceptibility measurements, and they are discussed in relation with the single-crystal X-ray diffraction data.

Experimental Section

Chemical Sources and Syntheses. Manganese(II) nitrate tetrahydrate, anhydrous lithium perchlorate, 2,2′-bipyrimidine (bpym), deuterated water, and 99% ^{15}N enriched potassium cyanide were purchased from commercial sources and used as received. All cyanide solutions were stored in the dark. The Li-*fac*-[Fe(L)-$(CN)_3]\cdot 4H_2O$ [L = $HB(pz)_3^-$ and $B(pz)_4^-$] salt and the corresponding C^{15}N containing derivative were prepared as previously described.[21]

Single crystals of **1**−**4** were grown by a slow diffusion technique using an H-shaped glass vessel. The starting materials were an aqueous solution of $Li[Fe(L)(CN)_3]\cdot 4H_2O$ at one arm (0.025 mmol) and a 1:1 mixture of $Mn(NO_3)_2\cdot 4H_2O$ and bpym (0.025 mmol) in water at the other one. Deuterated water was used as solvent in the preparation of **4**. Red prismatic crystals were formed after 2 weeks. The crystals were collected and dried on filter paper. Yield: about 50% for **1**−**4**. Elemental analyses (C, H, N) were performed by the SIARE at the Université Paris 6. Calcd for $C_{64}H_{56}B_4Fe_4Mn_2N_{44}O_2$ (**1**): C, 41.55; H, 3.05; N, 33.31. Found: C, 40.70; H, 3.18; N, 31.90%; C $_{76}H_{72}B_4Fe_4Mn_2N_{52}O_6$. Calcd for (**4**): C, 41.75; H, 3.32; N, 33.32. Found: C, 43.40; H, 3.39; N, 33.89%; (the enriched compounds **2** and **3** were prepared in such small amounts that their composition was established by X-ray diffraction on single crystals).

Caution*! Perchlorate salts are potentially explosive. Although no problems were experienced with the compounds used, they should only be handled in small quantities, neither scraped from sintered glass frits nor heated in the solid state. Waste solutions containing cyanide were treated with basic solutions containing hypochlorite to transform cyanide into cyanate.*

Crystal Structure Data Collection and Refinement. Diffraction data were obtained from a Bruker KAPPA CCD area-detector diffractometer (ω and φ rotation scans with narrow frame) equipped with graphite monochromated Mo Kα radiation (λ = 0.71073 Å). The data were corrected for Lorentz polarization effect and for the effects of absorption by multiscan method using SADABS [G.M. Sheldrick, SADABS, University of Göttingen, Germany, 1997]. The non-hydrogen atoms were refined anisotropically. The hydrogen atoms were located with geometrical restraints in the riding mode. The cell parameters for **1**−**4** at different temperatures are listed in Table 1. Crystal data for **1a** ($C_{64}H_{56}B_4Fe_4Mn_2N_{44}O_2$): T = 295(2) K, $P\bar{1}$, Z = 1, μ = 1.051 mm^{-1}, ρ_{calc} = 1.49 g cm^{-3}, 27977 reflections measured (θ_{max} = 30.00°), 11788 unique (R_{int} = 0.05) and of these 5597 had $I > 3\sigma(I)$. The values of the final residuals R_1 and wR_2 were 0.037 and 0.038 respectively for 542 parameters. Crystal data for **1b** ($C_{64}H_{56}B_4Fe_4Mn_2N_{44}O_2$): T = 200(2) K, $P2_1/a$, Z = 2, μ = 1.069 mm^{-1}, ρ_{calc} = 1.51 g cm^{-3}, 25800 reflections measured (θ_{max} = 30.02°), 11120 unique (R_{int} = 0.06) and of these 5363 had $I > 3\sigma(I)$. The values of the final residuals R_1 and wR_2 were 0.040 and 0.042, respectively for 542 parameters. The crystallographic axes x, y, and z in **1a** are converted into $-y$, $-z$ and x, respectively, in **1b**. Crystal data for **2a** ($C_{64}H_{56}B_4Fe_4Mn_2N_{44}O_2$): T = 295(2) K, $P\bar{1}$, Z = 1, μ = 1.045 mm^{-1}, ρ_{calc} = 1.48 g cm^{-3}, 22848 reflections measured (θ_{max} = 30.00°), 11798 unique (R_{int} = 0.05) and of these 4730 had $I > 3\sigma(I)$. The values of the final residuals R_1 and wR_2 were 0.038 and 0.037, respectively for 542 parameters. Crystal data for **2b** ($C_{64}H_{56}B_4Fe_4Mn_2N_{44}O_2$): T = 200(2) K, $P2_1/a$, Z = 2, μ = 1.068 mm^{-1}, ρ_{calc} = 1.51 g cm^{-3}, 59437 reflections measured (θ_{max} = 30.00°), 11826 unique (R_{int} = 0.06) and of these 6406 had $I > 3\sigma(I)$. The values of the final residuals R_1 and wR_2 were 0.059 and 0.068, respectively, for 543 parameters. The crystallographic axes x, y, and z in **2a** are converted into $-y$, $-z$, and x, respectively in **2b**. Crystal data for **3** ($C_{64}H_{52}D_4B_4Fe_4Mn_2N_{44}O_2$): T = 200(2) K, $P\bar{1}$, Z = 1, μ = 1.055 mm^{-1}, ρ_{calc} = 1.49 g cm^{-3}, 34887 reflections measured (θ_{max} = 27.5°), 9413 unique (R_{int} = 0.06) and of these 5463 had $I > 3\sigma(I)$. The values of the final residuals R_1 and wR_2 were 0.033 and 0.032, respectively for 542 parameters. Crystal data for **4** ($C_{76}H_{72}B_4Fe_4Mn_2N_{52}O_6$): T = 200(2) K, $P\bar{1}$, Z = 1, μ = 0.911 mm^{-1}, ρ_{calc} = 1.49 g cm^{-3}, 45127 reflections measured (θ_{max} = 30.00°), 13879 unique (R_{int} = 0.06) and of these 7963 had $I > 3\sigma(I)$. The values of the final residuals R_1 and wR_2 were 0.039 and 0.042, respectively for 650 parameters.

FT-IR Spectroscopy. The FT-IR spectra were recorded as KBr pellets in the 400−4000 cm^{-1} region. Room temperature measurements of all compounds were carried out using a Bruker Tensor 27 FTIR spectrophotometer. For all these spectra, 32 scans were averaged at a 4 cm^{-1} resolution. Variable-temperature measurements of **1a**−**1b** were carried out on a Nicolet6700 apparatus equipped with a cryostat. For all spectra, 32 scans were averaged at a 2 cm^{-1} resolution. After the spectra were recorded at 300 K, the temperature was reduced down to 130 K with a helium compressor. Then, the compressor was switched off, and the spectra were recorded in the heating regime from 130 to 300 K. The temperature heating rate was maintained between 0.5 and 1 K min^{-1}.

Optical Reflectivity. Surface reflectivity measurements were performed on a home-built system at temperatures ranging from 10 to 300 K. Heating and cooling rates have been maintained at 4 K min^{-1} during the measurements. This setup collects the light reflected by the sample (that is the sum of direct and diffuse reflected light) that is analyzed by a high sensitivity Hamamatsu 10083CA spectrometer between 400 and 1000 nm. The spectra were measured with a Leica CLS 150 XD tungsten halogen source, which is adjustable at 50 μW cm^{-2} onto the sample. The spectra are compared to a white reference obtained with a NIST traceable standard for reflectance (sphereOptics, ref SG3054). The background, which is the spectrum acquired with the light source switched off, is subtracted from all measurements. The reflectivity can be plotted as a function of either temperature, time, or wavelength.

Magnetic Measurements. Magnetic susceptibility measurements on polycrystalline samples of **1**, **3**, and **4** were carried out

(21) Costa, V.; Lescouëzec, R.; Vaissermann, J.; Herson, P.; Journaux, Y.; Araujo, M. H.; Clemente-Juan, J. M.; Lloret, F.; Julve, M. *Inorg. Chim. Acta* **2008**, *361*, 3912.

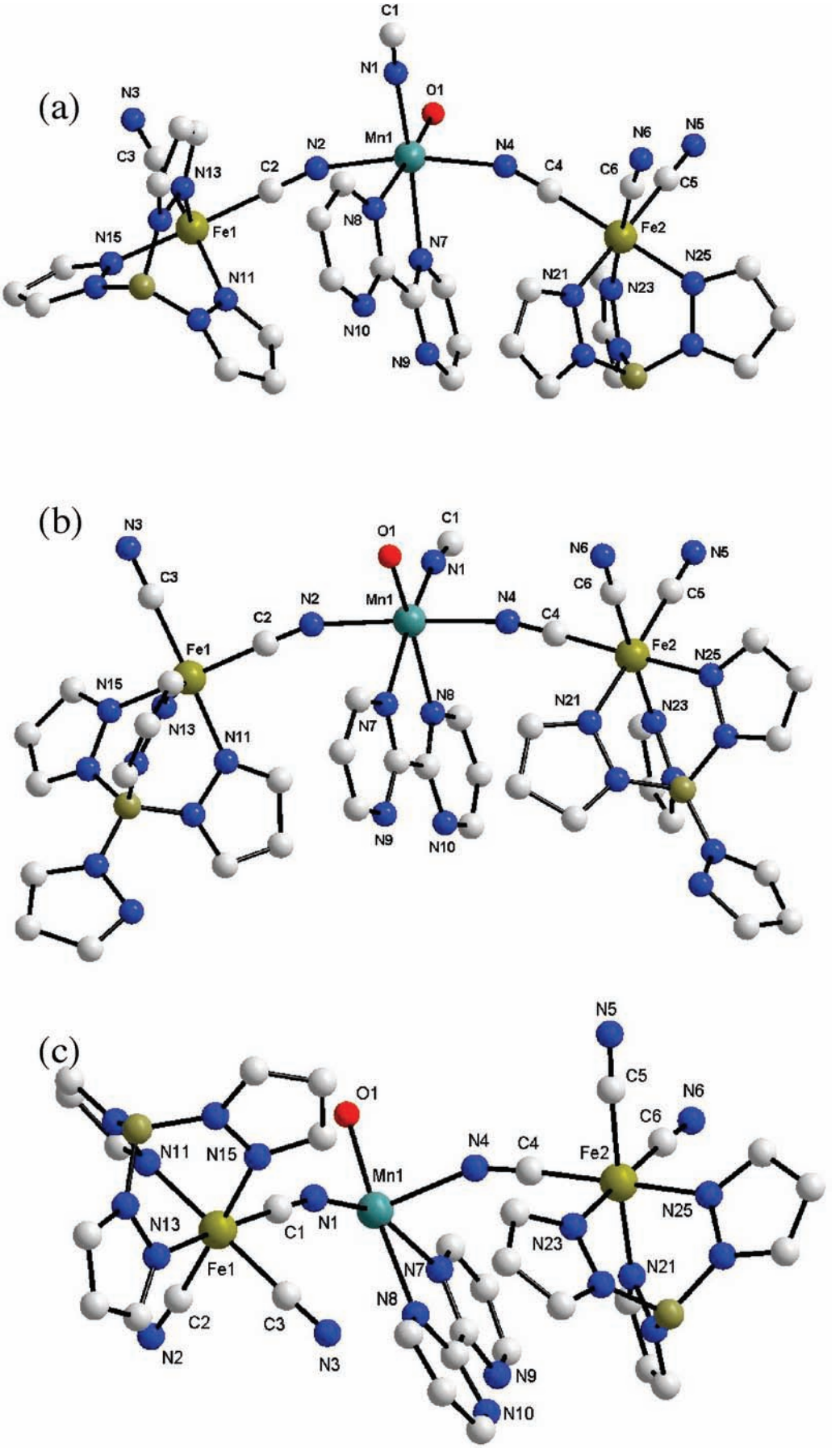

Figure 1. Views of the asymmetric unit of **1a**, **2a**, and **3** (a), **1b** and **2b** (b), and **4** (c) together with the atom numbering scheme.

with a Superconducting Quantum Interference Design (SQUID) magnetometer in the temperature range 1.9−300 K and under an applied field ranging from 250 to 2500 G. The temperature was swept using a 2 K min^{-1} rate on both heating and cooling measurements of **1**, **3**, and **4**. Additional magnetic experiments were carried out on **1** between 300 and 100 K with a sweep-rate as small as 0.05 K min^{-1} to detect the structural phase transition. All the magnetic susceptibility data were corrected for the diamagnetic contribution of the constituent atoms through the Pascal constants [-727×10^{-6} (**1** and **3**) and -884×10^{-6} cm^3 mol^{-1} (**4**) per $Fe^{III}{}_4Mn^{II}{}_2$ unit][22] and also for the sample holder.

Results

Solid State Structure Analysis. X-ray diffraction measurements on dark-red single crystals of **1**−**4** were performed in the temperature range 300−95 K. At room temperature, all four compounds crystallize in the $P\bar{1}$ space group. **1**, **2**, and **3** are isostructural, and their structures resemble that of **4** (Table 1). **3** and **4** maintain the room temperature structure in the explored temperature range, whereas **1** and **2** undergo a structural phase transition around 200 K. Hereafter, the room temperature phases of **1** and **2** will be referred as **1a** and **2a** and the low temperature ones as **1b** and **2b**.

A view of the asymmetric units for **1a**, **2a**, **3**, and **4** is shown in Figure 1. Angles, bond distances, and crystal structure parameters in **1a** and **2a** (at 295 K) and in **3** and **4** (at 200 K) are given in the Supporting Information. **1a**, **2a**, **3**, and **4** are made up of centrosymmetric $Fe^{III}{}_4Mn^{II}{}_2$ hexanuclear entities including two types of $[Fe(L)(CN)_3]^-$ units [iron atoms noted Fe(1) and Fe(2)]: one of them [Fe(2)] acting as a terminal monodentate ligand and the other one [Fe(1)] adopting a bis-monodentate bridging mode toward the $[Mn(1)(bpym)(H_2O)]^{2+}$ units through cyanide groups (Figure 2a). The resulting molecular structure has a central $[Fe^{III}{}_2Mn^{II}{}_2(\mu\text{-}CN)_4]^{6+}$ quasi-square planar core [Fe(1)···Mn(1) and Fe(1)···$Mn(1)^i$ distances of 5.230(1) and 5.192(1) Å in **1a**, 5.241(1) and 5.202(1) Å in **2a**, 5.228(1) and 5.193(1) Å in **3**, 5.235(1) and 5.200(1) Å in **4**; symmetry code: (i) = $-x, -y, -z$], and two pendant $[Fe^{III}(L)(CN)_3]^-$ units in *trans* position [Fe(2)···$Mn(1)^i$ = $Fe(2)^i$···Mn(1) = 5.159(1), 5.173(1), 5.151(1), and 5.219(1) Å for **1a**, **2a**, **3**, and **4**, respectively]. The metal atoms in **1**−**4** are six-coordinated adopting distorted octahedral coordination surroundings including three pyrazolyl-nitrogen and three cyanide-carbon atoms at the Fe(1) and Fe(2) metal centers and two nitrogen atoms from a bidentate bpym ligand, a water molecule, and three cyanide-nitrogen atoms in a *mer* arrangement at the Mn(1) site. The values of the Fe−C distances vary in a narrow range for all the compounds [1.915(4)−1.954(4) Å], and they are in agreement with those observed in previous examples of structurally characterized low-spin iron(III) mononuclear complexes containing the *fac*-$\{[Fe^{III}\{HB(pz)_3\}(CN)_3]^-$ anion [1.910(6)−1.930(3) Å].[9b,23] The Fe−N bond lengths span also in the very narrow range of 1.968(3)−1.999(3) Å, and they are significantly shorter than those found in the high-spin iron(III) complex *fac*-$[Fe\{HB(pz)_3\}Cl_3]^-$ [2.152(4)−2.175(5) Å].[24]

The values of the Mn−O [2.124(2)−2.142(2) Å], Mn−N(CN) [2.199(2)−2.239(4) Å], and Mn−N(bpym) [2.329(2)−2.360(3) Å] bond distances are very similar in the four compounds **1a**, **2a**, **3**, and **4**. The main distortion in the N_5O octahedral environment at the Mn site arises from the bite angle of the chelating bpym ligand [70.70(10)−71.22(9)°]. All Mn−N−C angles deviate notably from linearity [155.30(30)−162.60(23)°] while the Fe−C−N angles are closer to 180° [values covering the range 174.5(3)−178.2(3)°]. The hexanuclear complexes in **1a**, **2a**, and **3** are interlinked along both *c* and *a* axes through hydrogen bonds leading to a two-dimensional (2D) supramolecular network (Figure 3a). Hydrogen bonds between the coordinated water molecule and one of the peripheral cyanide ligands [O(1)···$N(6)^{ii}$ = 2.743(6) (**1a**), 2.744(7) (**2a**), and 2.752(8) Å (**3**); symmetry code: (ii) = $1 - x, 2 - y, -z$] build a uniform chain of hexameric motifs along the crystallographic *c* axis (Figure 2b). Weaker hydrogen bonds involving the coordinated water molecule and a free bpym-nitrogen atom from a neighboring complex [O(1)···$N(10)^{ix}$ = 2.958(4) (**1a**), 2.965(4) (**2a**), and 2.930(3) Å (**3**); symmetry code: (ix) = $x - 1, y, z$] lead to a second type of supramolecular chain along the crystallographic *a* axis. These features together with the values of the N−O−N angles [$N(6)^{ii}$−O(1)−$N(10)^{ix}$ = 121.1(1) (**1a**), 121.2(2) (**2a**) and 121.0(2)° (**3**)] are compatible with the coexistence of both types of hydrogen bonds. The shortest intermolecular metal−metal distances are found along both H-bond directions: Fe···Mn = 7.064(1), 7.075(1), and 7.080(1) Å and Mn···Mn (= Fe···Fe) = 8.804(1), 8.817(1), and 8.727(1) Å in **1a**, **2a**, and **3**, respectively. The shortest intermolecular metal−metal distances in **4** are significantly longer [Fe···Mn = 8.750(1) Å, Mn···Mn = 8.856(1) Å, and Fe···Fe = 8.343(1) Å] and two additional crystallization water molecules [O(200) and O(300)] are hydrogen bonded to the coordinated water [(O(100)]. These lattice solvent molecules are themselves linked to neighboring hexanuclear units (Figures 4b and 4c). Indeed, O(200) forms a hydrogen bond with a free bpym-nitrogen atom whereas O(100) is involved in a hydrogen bond with two uncoordinated nitrogen atoms belonging to the fourth uncoordinated pyrazolyl group from two neighboring units [O(1)···O(200) = 2.749(4) Å, O(1)···O(100) = 2.676(4) Å, O(200)···N(9)′ = 2.857(4) Å, O(100)···N(18)″ = 2.912(4) Å, and O(100)···N(28)‴ = 2.949(4) Å [symmetry code: (′) = $1 + x, y, z$, (″) = $1 - x, 1 - y, 1 - z$ and (‴) = $2 - x, 1 - y, -z$]. This hydrogen bonding patterns leads thus to a H-bonded chain of hexanuclear units along the crystallographic *a* axis. Overall, a supramolecular 2D network of hexanuclear complexes results, which grows in the *ac* plane.

While **3** and **4** maintain the same structure in all the explored temperature range (300−95 K), the situation is different for **1** and **2**. During the X-ray crystallographic measurements of **1**, new diffraction spots appear around 215 K upon cooling from room temperature at about 1 K min^{-1}. When the temperature is maintained at least 2 h at 200 K, the intensity of the diffraction peaks does not vary anymore, and a new crystal structure can be determined in the $P2_1/a$ space group. This thermal behavior is characteristic of structural phase transition (from **1a** in $P\bar{1}$ at high temperature to **1b** in $P2_1/a$ at low temperature) also called a SCSC phase transition. No other structural changes are observed down to 95 K (the lowest available

(22) Bain, G. A.; Berry, J. F. *J. Chem. Educ.* **2008**, *85*, 532.
(23) Kim, J.; Han, S.; Cho, I.-K.; Choi, K. Y.; Heu, M.; Yoon, S.; Suh, B. J. *Polyhedron* **2004**, *23*, 1333.
(24) Kukui, H.; Ito, M.; Morooka, Y.; Kitajima, N. *Inorg. Chem.* **1990**, *29*, 2868.

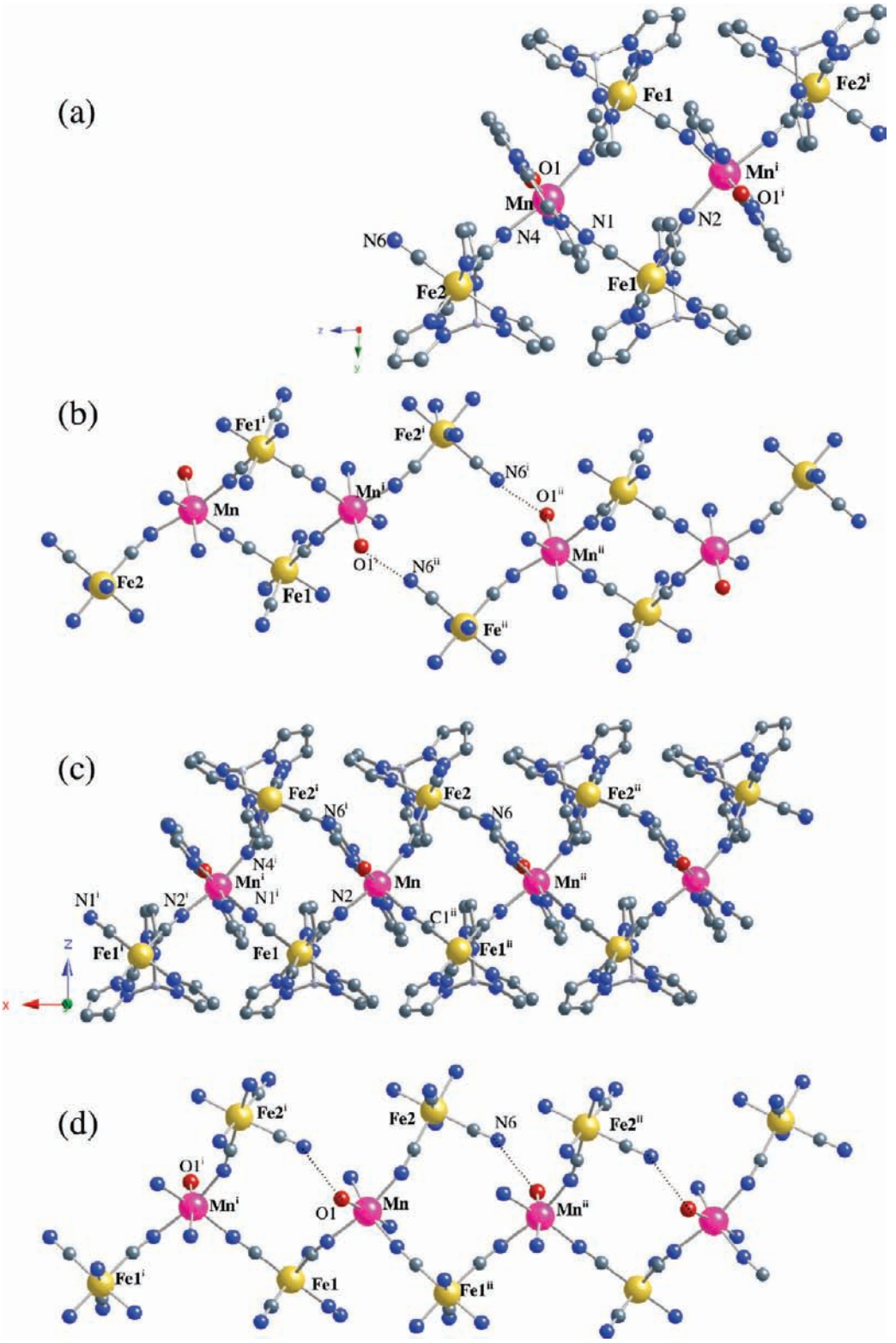

Figure 2. Structure of $\{[Mn(bpym)(H_2O)]_2[Fe(HB(pz)_3)(CN)_3]_4\}$ at 295 [(a) and (b)] (**1a**) and 200 K [(c) and (d)] (**1b**): view of the hexanuclear unit (a) and of the skeletons of two neighboring hexanuclear units connected through hydrogen bonds (dotted lines) along the *c* axis in **1a** (b) [Symmetry code: (i) $= -x, -y, -z$; (ii) $= x, y, z+1$]; view of the chain running along the *a* axis (c) and of the skeleton of the chain arrangement in **1b** (d) [Symmetry code: (i) $= x+1/2, -y-1/2, z$; (ii) $= x-1/2, -y-1/2, z$]. The hydrogen atoms were omitted for clarity in (a)−(d) while the pyrazolyl ligands are additionally omitted in (b) and (d).

temperature). Upon warming (at about 1 K min^{-1}), diffraction spots of the high temperature phase appear around 190 K, and the high temperature phase is fully recovered at 300 K. Similarly, compound **2a** undergoes a structural phase transition around 200 K that transforms the high temperature phase **2a** into **2b** at low temperature. **1b** and **2b** are isostructural compounds whose structure is made up of zigzag chains in which

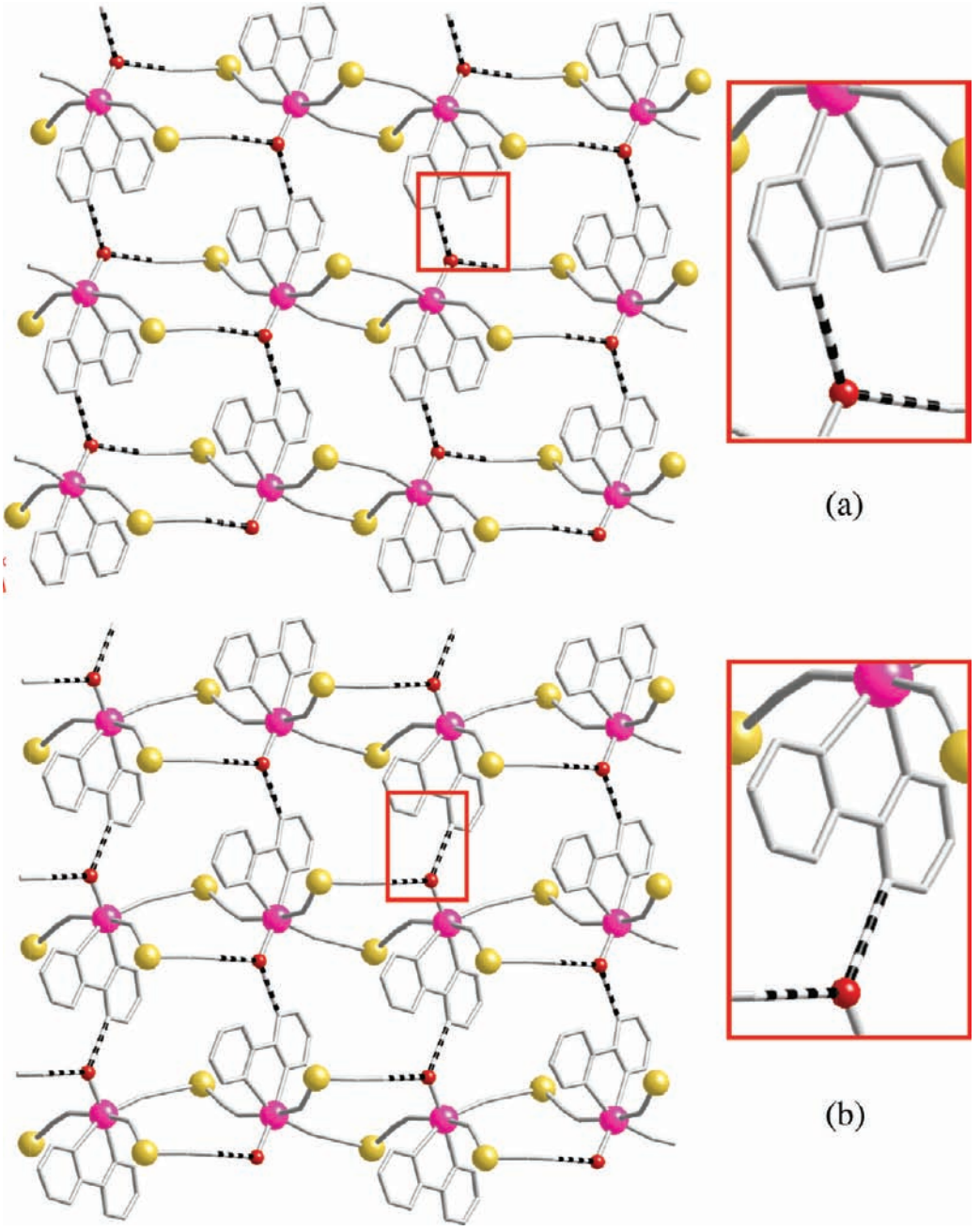

Figure 3. (a) View of the hydrogen bond network in the *ac* plane for **1a**, **2a**, and **3** (a) and **1b** and **2b** (b) together with a detail of the hydrogen bond involving the bpym ligand (right). (b) View of the hydrogen bond network in **1b** and **2b** in the *ac* plane together with a detail of the hydrogen bond involving the bpym ligand (right). The hydrogen atoms and the pyrazolyl ligands were omitted for clarity.

two $[Fe(1)^{III}\{HB(pz)_3\}(CN)_3]^-$ units act as bis-monodentate ligands toward the $[Mn(H_2O)(bpm)]^{2+}$ motifs. An additional pending $[Fe(2)^{III}\{HB(pz)_3\}(CN)_3]^-$ complex which acts as a monodentate ligand fills the sixth coordination position at the manganese(II) ion (Figure 2c). The Fe(III) and Mn(II) ions in **1b** and **2b** retain their slightly distorted octahedral FeC_3N_3 and MnN_5O environments, and no significant changes in the values of the bond lengths are observed respect to those in **1a** and **2a**. The Fe−C and Fe−N bond distances still vary in a narrow range [1.928(5)−1.958(4) and 1.988(3)−1.997(3) Å, respectively]. The coordination bonds around the manganese(II) ion are also very close to those observed at higher temperature [Mn−O = 2.141(3)−2.147(3) Å, Mn−N(CN) = 2.220(3)−2.250(4) Å and Mn−N(bpym) = 2.341(3)−2.349(3) Å]. The main distortion from the octahedral geometry arises from the bite angle of the chelating bpym ligand [70.5(1)° (**1b**) and 70.8(1)° (**2b**)]. The cyanide bridges are bent on the Mn side [the Mn−N−C angles varying between 154.9(3)° and 168.3(3)°] whereas those of the Fe−C−N angle are closer to linearity [176.3(3)−179.2(4)°]. Only the values of the Fe(1)−C(2)−N(2) angle decrease slightly to 172.2(3)° and 171.9(4)° for **1b** and **2b**, respectively. The metal−metal distances (equal in **1b** and **2b**) across the cyanide bridges are therefore close to those observed in the high temperature phase [Fe(1)···Mn(1) = 5.294(1) Å, Fe(1)···Mn(1)^{i} = 5.194(1) Å and Fe(2)···Mn(1) = 5.181(1) Å; symmetry code: (i) = $0.5 + x, 0.5 - y, z$]. In addition, it is worth noting the short metal to

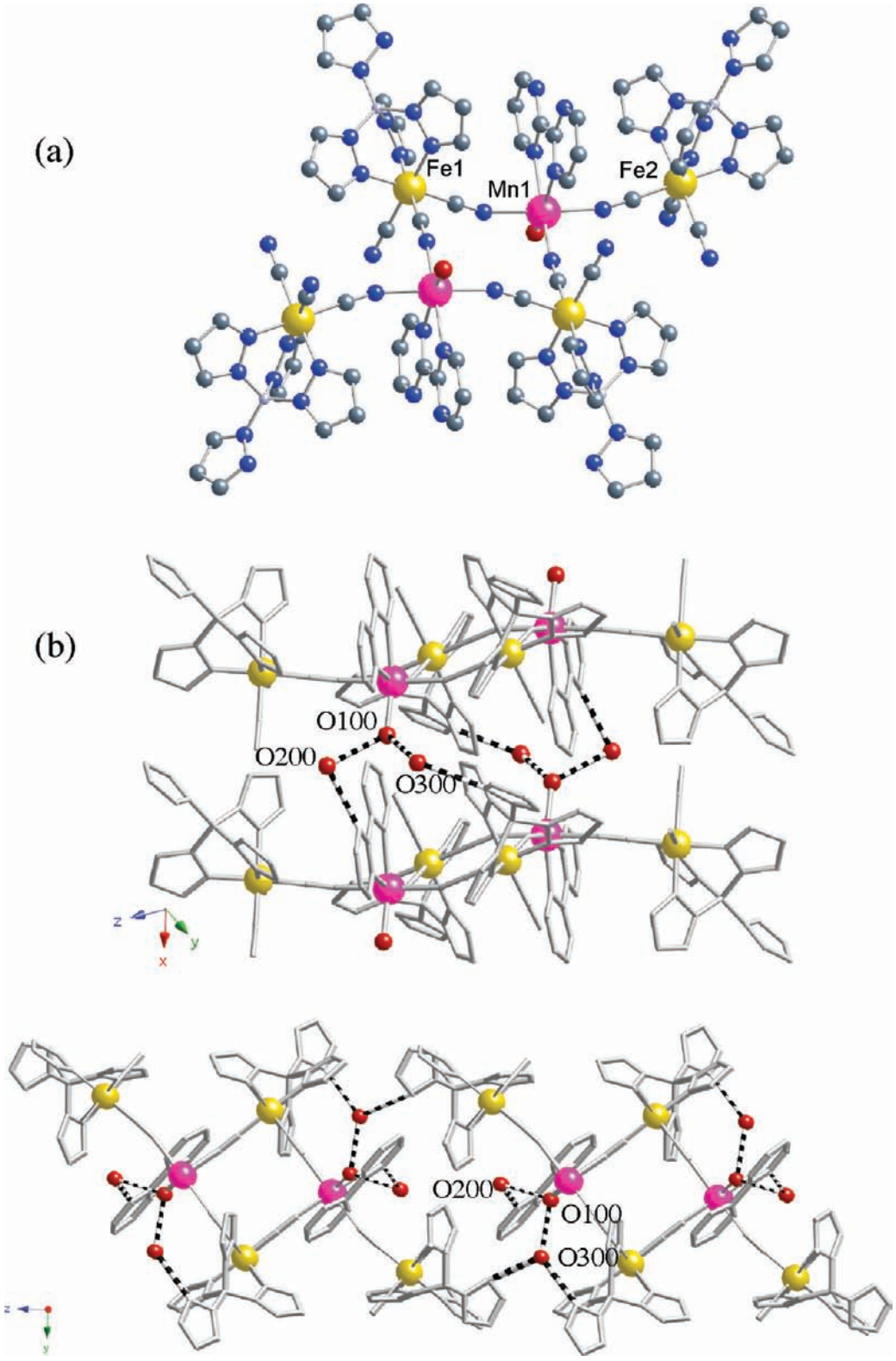

Figure 4. Structure of $\{[Mn(bpym)(H_2O)]_2[Fe(B(pz)_4)(CN)_3]_4\}\cdot 4H_2O$ (**4**): view of the hexanuclear unit (a) and of its interconnection through hydrogen bonds along the *a* (b) and *c* (c) crystallographic axes.

metal distances along the Fe(2)−C(6)−N(6)···O(1)−Mn(1) pathway [Fe(2)−Mn(1)^{i} = 6.886(1) and 6.891(1) Å] where the coordinated water molecule is linked to one of the terminal cyanide of a Fe(2) unit through a hydrogen bond [N(6)···O(1)^{i} = 2.786(5) and 2.780(7) Å in **1b** and **2b**, respectively; symmetry code: (i) = $x - 0.5, -y + 1.5, z$] (Figure 2d). The coordinated water molecule is also involved in a somehow weaker hydrogen bond with one free bpym-nitrogen atom from a neighboring chain [N(10)^{ii}···O(1) = 2.978(5) (**1b**) and 2.977(7) Å (**2b**); symmetry code: (ii) = x, $1 + y$, z] leading thus to a hydrogen bonded 2D network (Figure 3b). The shortest

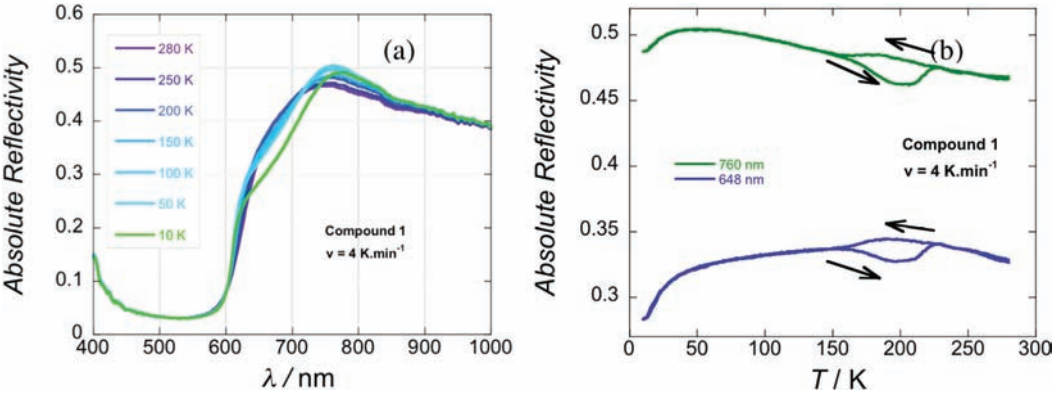

Figure 5. (a) Selected surface reflectivity spectra under white light irradiation (50 μW cm^{-2}) of **1** with cooling from 280 to 10 K (4 K min^{-1}). (b) Absolute reflectivity of **1** at 760 nm (green) and 648 nm (blue) under cooling and heating.

metal−metal interchain distances are 8.832(1) (Mn···Mn = Fe···Fe) and 8.975(1) Å (Mn···Fe).

FT-IR spectra of **1**−**4** have been recorded at room temperature in the range 400−4000 cm^{-1}. Several IR vibrations account for the presence of the organic blocking ligands. Characteristic bands of the $HB(Pz)_3^-$ group including those at 1500s, 1405s, 1311s, 1210s, 1045s cm^{-1} are present in the FT-IR spectra of **1**−**3**. **4** exhibits similar vibrations together with those at 1501 m, 1409s, 1307s, 1214 m, 1063s cm^{-1}. They compare well with those observed in the IR spectrum of the $K[B(Pz)_4]$ salt. The peak located at 2515w cm^{-1} in **1**−**3** is unambiguously attributed to the presence of a B−H bond (stretching vibration). Moreover, the vibrations at 1571 m and 1558 m cm^{-1} (symmetric aromatic ring stretching modes) account for the presence of the bidentate bpym ligand in **1**−**4**. The cyanide stretching vibrations are informative of both the coordination mode of the cyanide ligands and the oxidation state of the connected metal ions. The weak peaks of the cyanide stretching vibration for **1a**, **3**, and **4** are located close to 2120 cm^{-1}, a value which remains close to those observed in the low-spin iron(III) building blocks (ca. 2123 cm^{-1}) and that accounts for the presence of non-bridging cyanide in them. The CN stretching vibrations move toward higher wavenumbers upon coordination to a second metal ion due the combined effects of dominant electron σ-donation and kinematic coupling in the M−CN−M′ fragments. The vibrations observed at 2144m (**1** and **3**) or 2140m cm^{-1} (**4**) together with a shoulder located at 2154m (**1** and **3**) or 2160m (**4**) cm^{-1} are therefore attributed to the presence of the three Fe^{III}−CN−Mn^{II} bridging cyanides. A significant isotopic effect is observed in **2a**. Whereas a single peak is observed at 2095 cm^{-1} in the complex $PPh_4[Fe^{III}\{HB(pz)_3\}(C^{15}N)]$ (PPh_4^+ = tetraphenylphosphonium cation), the vibrations at 2093w and 2114m cm^{-1} are assigned to non-bridging and bridging cyanide ligands, respectively.

The temperature dependence of the FT-IR spectra of **1** has been studied in the available temperature range 130−300 K (Supporting Information, Figure S1). A FT-IR spectrum was first recorded at room temperature before cooling the sample down to 130 K (the spectra were recorded upon warming because the compressor vibrations in our setup prevent us from measuring during the cooling process). Whereas all the observed IR vibrations slightly decrease with a maximal deviation of about 1 cm^{-1} as the temperature increases (0.5−1 K min^{-1} heating rate), those attributed to bridging cyanide shift more significantly from 2147.7 to 2144.0 cm^{-1} and from 2159.3 to 2154.4 cm^{-1}. Both spectra performed at room temperature are identical. As shown in Figure 5, the thermal shifts of the IR vibrations are continuous, and no anomaly is observed between 130 and 290 K that could be related to a phase transition around 200 K, as observed by single-crystal X-ray diffraction studies.

Optical Reflectivity Studies. Solid-state reflectivity spectra for **1**, **3**, and **4** have been collected between 280 and 10 K (under white light irradiation, 0.05 mW cm^{-2}). It is worth noting that the physical properties of the ^{15}N compound **2** are not reported in this work because of the difficulty to prepare a sufficient amount of sample.

At 280 K, the spectra are composed on a broad absorption band below 600 nm, which is centered around 500 nm (Figure 5a and Supporting Information, Figure S2). With cooling, the spectra exhibit only small changes down to 50 K. Below 50 K, a new spectral feature located around 700 nm appears. Upon heating, this band disappears again, and the spectrum at 280 K is similar to the ones obtained before the thermal cycle. An alternative way to visualize these optical changes with the temperature, is to follow the thermal dependence of the absolute reflectivity at selected wavelengths, here 648 and 760 nm (hereafter noted R_{648} and R_{760}). The three compounds present different thermal behaviors. Whereas the data collected in the cooling and heating modes are perfectly superimposed for **3** and **4** (Supporting Information, Figures S3 and S4), the situation is obviously different for **1** (Figure 5). Upon cooling, an increase in R_{648} is observed for **1**, changing significantly from 0.33 at 280 K to 0.35 at 200 K (Figure 5a) while at lower temperatures, R_{648} decreases toward 0.28 at 10 K. Upon heating, R_{648} starts to increase to 0.33 at 158 K, then decreases to a value of 0.34 at 200 K, and finally increases slightly to recover the same value of 0.33 at 280 K. As shown in Figure 5b, a reproducible thermal hysteresis between 158 and 223 K is revealed in the 600−800 nm range. This thermal hysteresis and the structural phase transition observed by single-crystal X-ray diffraction occur in the same temperature range for **1** while both experimental studies coherently confirm the absence of any phase transition in **3** and **4**.

A last comment about these optical reflectivity measurements concerns the appearance below 50 K of a new

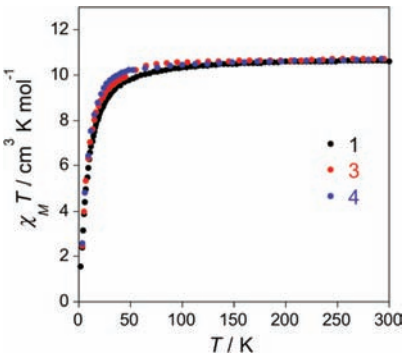

Figure 6. Temperature dependence of the $\chi_M T$ product (χ_M being the molar magnetic susceptibility normalized by [Fe_4Mn_2] units) of **1**, **3**, and **4** under a dc field of 0.1 T.

band around 700 nm in the three studied compounds (Figure 5, Supporting Information, Figures S2−S4). This thermally induced feature is therefore independent on the structural transition, and might be similar to the bands observed in the charge-transfer photomagnetic $Rb^{I}Mn^{II}$-Fe^{III} PBAs.[25] Therefore by analogy to these three-dimensional (3D) systems, photoexcitation properties of **1**, **3**, and **4** have been checked by cooling the samples to 10 K in the dark before light irradiation. Irradiations at 450, 550, and 650 nm (with a power of a few mW cm^{-2}) showed no significant changes of the optical spectra suggesting that these compounds are not photosensitive.

Magnetic Measurements. The magnetic properties of polycrystalline samples of **1**, **3**, and **4** have been investigated in the temperature range 2−300 K under a 0.1 T direct current (dc) magnetic field. The $\chi_M T$ versus T plots of **1**, **3**, and **4** are shown in Figure 6 (χ_M being the molar magnetic susceptibility per [$Fe^{III}{}_4Mn^{II}{}_2$] unit). Curiously, all curves show a similar shape, which corresponds to an overall antiferromagnetic behavior. The values of the $\chi_M T$ product at room temperature (10.6−10.7 cm^3 K mol^{-1}) are in good agreement with the expected value for uncoupled spin carriers: a set of four low-spin iron(III) ions and two high-spin manganese(II) ions (ca. 10.25 cm^3 K mol^{-1} for spin only value with $g = 2$). Upon cooling, the $\chi_M T$ value slightly decreases between 300 and 50 K, and then more abruptly, reaching a value of about 1.6 cm^3 K mol^{-1} at 2.0 K. The slow and continuous decrease of $\chi_M T$ observed in **1**, **3**, and **4** at high temperatures is due to the spin−orbit coupling of the $^2T_{2g}$ ground term of the six-coordinated low-spin iron(III) centers, as observed in the precursor complex PPh_4[Fe{$HB(pz)_3$}-$(CN)_3$].[21] The decrease observed at lower temperatures is mainly attributed to weak intramolecular antiferromagnetic interactions between the low-spin iron(III) and the manganese(II) ions across the cyanide bridge. The lack of the predicted minimum of the $\chi_M T$ product for a ferrimagnetic chain in **1** is most likely due to the occurrence of significant interchain antiferromagnetic interactions. It is worth noting that the magnetic properties of the three compounds have been studied under the cooling and heating modes without showing differences whatever the temperature sweeping rate of the cooling/heating mode (additional magnetic measurements were carried out by introducing the sample at low temperatures, 200 and 10 K, and by measuring the magnetization over 3 h, but no significant variations of the $\chi_M T$ product have been observed).

Discussion

Remarkably, **1** and **2** exhibit a structural phase transition from $P\bar{1}$ to $P2_1/a$ around 200 K, the hexanuclear complex in **1a** and **2a** becoming a bimetallic chain in **1b** and **2b** (Figure 2) whereas **3** and **4** keep their hexanuclear topology down to 95 K (the lowest available temperature for our X-ray equipment). H-bonding reorganizations have often been observed in solid state,[26] but as described above, the present structural transition involves a unusual reorganization of both coordination and hydrogen bond networks. On one side, one of the two bridging cyanide group [C(1)N(1)] in **1a** and **2a** "leaves" the manganese ion, while the coordinated water molecule undergoes a displacement toward that "leaving" group to form a new hydrogen bond [N(6)···O(1) = 2.786(4) and 2.780(4) Å in **1b** and **2b**, respectively]. On the other side, the C(6)N(6) cyanide ligand from a neighboring complex that forms a hydrogen bond with the coordinated molecule in **1a** and **2a**, enters in the coordination sphere of the manganese ions in **1b** and **2b**. Overall, the manganese(II) ion maintains its coordination sphere during the structural transition. The preservation of the crystal quality during such demanding topological change of the structure is a quite relevant feature. The concerted reorganization of the coordination bonds and hydrogen bonds in the manganese coordination sphere is accompanied by other modifications in the hydrogen bond network in the crystal lattice. Indeed, the coordinated water molecule, which forms a second hydrogen bond with the peripheral uncoordinated nitrogen atoms of the bpym ligand, switches from one peripheral nitrogen atom to the other as this water molecule undergoes a displacement (Figure 3) [N(10)···O(1) = 2.978(5) and 2.977(7) Å in **1b** and **2b**, respectively]. The N−O−N angles in the two phases are compatible with the coexistence of both hydrogen bonds [N(6)O(1)N(10) = 124.97(13) and 125.20(15)° in **1b** and **2b**, respectively]. This topo-chemical reaction can also be described as a "complex-as-ligand" exchange: while one [Fe(2){HB-$(pz)_3$}$(CN)_3$]$^-$ bridging unit of the hexanuclear molecule is disconnected to become a pending group of the final chain, the [Fe(1)[$HB(pz)_3$]$(CN)_3$]$^-$ pending units of the neighboring hexanuclear molecules (located in *trans* position) get coordinated to the manganese(II) ion to become a bridging unit along the chain. This results in the formation of a zigzag chain where one [Fe(1){$HB(pz)_3$}$(CN)_3$]$^-$ unit acts as a bis-monodentate ligand toward the manganese site and another one, [Fe(2){$HB(pz)_3$}$(CN)_3$]$^-$, acts as a monodentate ligand toward the manganese(II) ion. Finally, the intramolecular metal−metal distances are slightly longer in **1b/2b** than in **1a/2a** [Fe(2)−C(1)N(1)−Mn = 5.294(1)/5.293(1) Å; Fe(1)−C(2)N(2)−Mn = 5.181(1)/5.182(1) Å, Fe(2)−C(4)N(4)−Mn = 5.194(1)/5.196(1) Å].

The properties of the compounds have been investigated using spectroscopic, optical, and magnetic techniques. On

(25) Tokoro, H.; Matsuda, T.; Nuida, T.; Moritomo, Y.; Ohoyama, K.; Davy Loutete Dnagui, E.; Boukheddaden, K.; Ohkoshi, S.-I. *Chem. Mater.* **2008**, *20*, 423.

(26) (a) Rau, S.; Ruben, M.; Büttner, T.; Temme, C.; Dautz, S.; Görls, H.; Rudolph, M.; Walther, D.; Brodkorb, A. *Dalton Trans.* **2000**, 3649. (b) Legrand, Y.-M.; Van der Lee, A.; Masquelez, N.; Rabu, P.; Barboiu, M. *Inorg. Chem.* **2007**, *46*, 9083.

one side, the FT-IR spectroscopic measurements and magnetic measurements of **1** do not provide any evidence of a phase transition between 2 and 300 K. On the other side, the optical reflectivity of **1** shows a clear thermal hysteresis associated with the observed structural phase transition. Even if these results seem in contradiction, a detailed examination of the structures in the different phases account for the whole set of experimental data. The structural transition corresponds to an exchange process of cyanide bonds, which consists of the leaving/entering C(1)N(1)/C(6)N(6) groups at the coordination sphere of the manganese(II) ion. Finally, between **1a** and **1b**, the ratio between the bridging and nonbridging cyanide groups per metal site is identical and therefore, no dramatic change is expected in the FT-IR spectra and magnetic properties during the structural transition. Actually, it is not surprising to find a similar magnetic behavior for the hexanuclear motif and the chain arrangement, as the strength and the number of magnetic exchange interactions do not change. Moreover, the exchange interaction between the high-spin Mn^{II} ($S = 5/2$) and low-spin ions through the cyanide ligand is known to be weak because of the compensation of the ferro- and antiferromagnetic contributions (ca. $J < 5\ cm^{-1}$).[27] The observation of the magnetic interactions is thus expected to be significant only at relatively low temperature whereas at higher temperature the magnetic behavior is close to the ones expected for non-interacting spins. It is worth noticing that previously reported compounds containing the $[Fe\{HB(pz)_3\}(CN)_3]^-$ unit and $Fe^{III}-CN-Mn^{II}$ bridges exhibit very similar magnetic behaviors despite their different topologies.[27b−d,28] In summary, although the spectroscopic and magnetic measurements carried out on **1** show serious limitations in detecting the structural phase transition, the single crystal diffraction experiment has allowed to reveal a rare case of thermally induced topochemical reaction. Concerning the optical reflectivity measurements, a thermal-induced hysteresis curve between 225 and 160 K is clearly associated to this phase transition. Although the coordination sphere of the manganese(II) ion is the same in **1a** and **1b**, the coordination bonds and their related angles exhibit small variations (Supporting Information, Tables S2, S3, S5, and S6). The optical reflectivity spectra are extremely sensitive to these small changes in the coordination spheres at the surface in the material and thus the transformation between **1a** and **1b** is easily observed with this technique.

Whereas ligand exchanges are well-known in solution and the molecules mobility may favor rearrangements, solid-state structural transitions with ligand exchange are quite uncommon. In this case and more generally in inorganic polymers, the SCSC phase transitions are even more seldom because only few topo-chemical reactions have been reported to preserve the integrity of the single crystals.[19] Their observation require several strict conditions, which appear to be fulfilled in the present case. First, the molecular components can rearrange only if they have flexibility. In **1**, the manganese-cyanide bond is labile enough so that the ligand exchange can occur. Such lability of the cyanide coordination bond in the solid state is somehow reminiscent of the linkage isomerization processes which have been evidenced in cyanide-containing three-dimensional polymers and molecular complexes.[29,30] Coordination bond reorganization has also been observed recently in another cyanide based complex, whose topology changes under the effect of solvent absorption/desorption, showing that this phenomenon is perhaps not so rare even if its observation stays uncommon.[31] Second, the topological rearrangements should be small. Here the cyanide groups involved in the connectivity changes are located at the "optimized" position to manage the structural changes. The C(6)N(6) cyanide ligand is placed close enough to the Mn^{II} metal ion through a short hydrogen bond in both high and low temperature phases. As a result, the corresponding "unlocked" Fe−Mn distances are only 7.064(1) Å in **1b** and 6.886(1) Å in **2b** [to be compared with 5.230(1) in **1a** and 5.294(1) Å in **2a** when "locked"]. The lack of phase transition in **4** allows an analysis of the topological requirements that govern the topo-chemical reaction. The use of a bulkier blocking ligand $[B(pz)_4]$ on the iron center and the presence of two additional crystallization water molecules in comparison with **1** and **2**, lead to a quite different supramolecular arrangement with longer intermolecular metal−metal distances that likely prevent the topological reorganization to occur. In **1** and **2**, the SCSC phase transition does not imply a strong displacement of the organic bulky component, both $HB(pz)_3$ and bpym ligands remaining close from their initial position. Therefore, it is likely that the two extra water molecules in the crystal packing (that probably increase the rigidity of the supramolecular network and reduce the available free space) are responsible for the absence of structural phase transition in **4**. The use of deuterated water in **3**, which forms weaker hydrogen bonds, precludes the observation of the thermo-induced phase transition, that is, on the other hand, unaffected by the use of ^{15}N enriched cyanide in **2**. In addition, it should be noticed that the topo-chemical reaction presented herein has only been observed with the manganese(II) derivatives. When using other divalent metal ions, either hexanuclear complexes or 1D compounds are obtained in the 95−300 K temperature range.[9c,32]

Conclusions

In this work, a rare case of SCSC reversible phase transition implying a concerted rearrangement of the coordination and hydrogen bonds and leading to a 0D−1D conversion is observed and studied in detail by structural, optical, spectroscopic, and magnetic techniques. In contrast with many other similar transitions, the present one is a reversible thermal-induced transition that involves exchange of cyanide ligands, and it does not imply any solvent absorption/desorption mechanism. So, the structural transformation occurs in the

(27) (a) Lescouëzec, R.; Lloret, F.; Julve, M.; Vaissermann, J.; Verdaguer, M. *Inorg. Chem.* **2002**, *41*, 818. (b) Wang, S.; Zuo, J.-L.; Zhou, H.-C.; Song, Y.; You, X.-Z. *Inorg. Chim. Acta* **2004**, *358*, 2101. (c) Kim, J.; Han, S.; Cho, I.; Choi, K. Y.; Heu, M.; Yoon, S.; Suh, B. J. *Polyhedron* **2004**, *23*, 1333. (d) Li, D.; Parkin, S.; Wang, G.; Yee, G.; Holmes, S. *Inorg. Chem.* **2006**, *45*, 1951.

(28) (a) Li, D.; Wang, G.; Yee, G. T.; Prosvirin, A. V.; Holmes, S. M. *Inorg. Chem.* **2005**, *44*, 4903–4905. (b) Kim, J.; Han, S.; Pokhodnya, I.; Migliori, J. M.; Miller, J. S. *Inorg. Chem.* **2005**, *44*, 6983. (c) Jiang, L.; Feng, X.-L.; Lu, T.-B.; Song, G. *Inorg. Chem.* **2006**, *45*, 5018.

(29) (a) Robin, M. B. *Inorg. Chem.* **1962**, *1*, 337. (b) Reguera, E.; Bertran, J. F.; Nunez, L. *Polyhedron* **1994**, *13*, 1619.

(30) (a) Shatruk, M.; Dragulescu-Andrasi, A.; Chambers, K. E.; Stoian, S. A.; Bominaar, E. L.; Achim, C.; Dunbar, K. R. *J. Am. Chem. Soc.* **2007**, *129*, 6104. (b) Long, J. R. *Chem. Commun.* **2007**, 1360.

(31) Ghosh, S. K.; Zhang, J.-P.; Kitagawa, S. *Angew. Chem., Int. Ed.* **2007**, 7965.

(32) Lescouëzec, R.; Armentano, D.; De Munno, G.; Lloret, F.; Julve, M., to be published.

whole bulk, and it does not depend on the propagation of molecules from the surface into the crystal lattice (or the other way). As suggested by recent results, such phenomenon may lead to new switchable molecular materials with flexible and dynamic frameworks that allow the tuning of their properties under the application of external stimuli (temperature, pressure, gas sorption, etc.).[19,33] Although the route to such materials seems to rely on serendipity, a better comprehension of the phase transition process and an improved control on the supramolecular organization through crystal engineering are the keys to design such systems. We are now searching for other magnetic systems which may exhibit such solid-state conversion, and whose magnetic properties should vary significantly in the two phases.

(33) See for example: (a) Biradha, M.; Fujita, M. *Angew. Chem., Int. Ed.* **2002**, *41*, 3392. (b) Niel, V.; Thompson, A. L.; Munoz, M. C.; Galet, A.; Goeta, A. E.; Real, J. A. *Angew. Chem., Int. Ed.* **2004**, *42*, 3760. (c) Toh, N. L.; Nagarathinam, M.; Vittal, J. J. *Angew. Chem., Int. Ed.* **2005**, *44*, 2937.

Acknowledgment. This work was supported by the Ministère de la Recherche et de l'Enseignement Supérieur (MRES), le Conseil National de la Recherche Scientifique (CNRS), the University of Bordeaux, the ANR (NT09_469563, AC-MAGnets project), the Region Aquitaine and the GIS Advanced Materials in Aquitaine (COMET Project) and the Ministerio Español de Ciencia y Tecnología through the Project CTQ2007-61690 and the Consolider Ingenio in Molecular Nanoscience CSD2007-0010.

Supporting Information Available: Additional structural parameters (Tables S1−S19), and additional FT-IR and UV−vis Figures (Figures S1−S4). This material is available free of charge via the Internet at http://pubs.acs.org. The CIF files are also available on application to the Cambridge Data Centre, 12 Union Road, Cambridge CB21EZ, U.K. (fax: (+44) 1223−336−033; e-mail: deposit@ccdc.cam.ac.uk), CCDC 787111 (**1a**), 787109 (**2a**), 787110 (**1b**), 787112 (**2b**), 787114 (**3**) and 787113 (**4**).